An Observational Study of Vortex Spacing in Island Wake Vortex Streets

GEORGE S. YOUNG AND JONATHAN ZAWISLAK

The Pennsylvania State University, University Park, Pennsylvania

(Manuscript received 21 June 2005, in final form 16 November 2005)

ABSTRACT

Vortex streets are a frequent occurrence in stratocumulus-topped flow downwind of mountainous islands. Theoretical studies dating back to von Kármán, supported by laboratory and numerical studies, have yielded similarity theories for the size and spacing of these vortices behind bluff bodies. Despite dynamical differences between such two-dimensional flows and the three-dimensional flow past isolated islands, satellite case studies suggest these geometric similarities may also hold for the atmospheric case. In this study, two of the resulting dimensionless ratios are measured using satellite imagery. One is the aspect ratio between cross-street and along-street spacing of the vortices. The second is the ratio of the cross-street spacing to the crosswind width of the island. A 30-image sample from the *Aqua* and *Terra* Moderate Resolution Imaging Spectroradiometer satellites is analyzed to obtain these ratios. The resulting set of values for the two dimensionless ratios is tested against the values found in bluff body studies. The aspect ratio is tested against the value of 0.28 resulting from von Kármán's inviscid theory, and the dimensionless width ratio is tested against the value of 1.2 from Tyler's laboratory study of flow around a bluff body. It is found that atmospheric vortex streets do indeed follow the geometric similarity theories, but with different values for the two ratios than those predicted by von Kármán and Tyler. The aspect ratio is larger than predicted as is the dimensionless width ratio. Both differences are consistent with the turbulent diffusion of vorticity in the wake of the island. The vortex streets more closely follow inviscid theory close to the island, with vortex expansion taking place a few vortex diameters downwind of the island.

1. Introduction

Satellite imagery frequently reveals striking patterns of mesoscale vortices in the atmospheric wakes downwind of mountainous islands as illustrated in Fig. 1 and Chopra and Hubert (1965), Chopra (1973), and Scorer (1986). Depending on the synoptic-scale wind and stability profiles, these island wakes can take the form of either a pair of counterrotating vortices trapped in the immediate lee of the island, or a train of vortices extending far downwind (Schär and Smith 1993a). These vortex trains bear a striking resemblance to those seen in high-Reynolds-number airflow around a bluff obstacle as described by von Kármán and Rubach (1912), leading many authors to suggest that they are the atmospheric analog of these von Kármán vortex streets. Decades of observational, theoretical, and modeling studies have gradually provided insight into the relationship between these two phenomena.

Island vortex streets have been observed from a number of satellites and manned spacecraft. Various Television Infrared Operational Satellites were used by Hubert and Krueger (1962), Chopra and Hubert (1965), and Chopra (1973), Environmental Science Services Administration satellites by Tsuchiya (1969) and Chopra (1973), a Nimbus satellite by Chopra (1973), a National Oceanic and Atmospheric Administration (NOAA) satellite by Thomson et al. (1977), and a Defense Meteorological Satellite Program satellite by Jensen and Agee (1978). The advantage of these polar-orbiting satellites over those in geosynchronous orbit is that image distortion by the curvature of the earth is minimized. Manned spacecraft have also been used to observe island-generated vortex streets: Mercury by Hubert and Krueger (1962), Gemini by Zimmerman (1969) and Chopra (1973), and Apollo by Chopra (1973). Chopra notes the severe image size limitations

Corresponding author address: Dr. George S. Young, 503 Walker Building, Meteorology Department, The Pennsylvania State University, University Park, PA 16802.
E-mail: young@meteo.psu.edu

FIG. 1. A von Kármán vortex street in the stratocumulus off the island of Guadalupe at 1845 UTC 13 Jun 2004. The image was taken by the *Terra* MODIS satellite. Image courtesy of MODIS Rapid Response Project at NASA GSFC.

of some of the early satellites and the problems this posed for determining vortex street length and thus vortex lifetime.

Island wake vortex streets have been seen almost exclusively in marine stratocumulus (e.g., reviews by Chopra 1973 or Etling 1989) downwind of steep islands that penetrate the inversion above cloud top (Chopra and Hubert 1965; Zimmerman 1969; Chopra 1973; Thomson et al. 1977). They can also form in the lee of clusters of such peaks, as observed by Thomson et al. (1977). Both cold-air outbreak stratocumulus under a frontal inversion (e.g., Jensen and Agee 1978; Thomson et al. 1977) and those under the trade wind inversion (e.g., Hubert and Krueger 1962; Chopra and Hubert 1965) provide suitable environments. The requirement for the island to penetrate the lid provided by a stratocumulus-capping inversion suggested to many of the early researchers a possible dynamical resemblance between these atmospheric vortex streets and those observed in two-dimensional flow behind a bluff body. In contrast, the high-resolution satellite imagery discussed below supports the more three-dimensional view of the near-island flow field that corresponds to the results of recent modeling studies.

The Moderate Resolution Imaging Spectroradiometer (MODIS; Platnick et al. 2003; King et al. 2003, 2004; see also information online at modis.gsfc.nasa.gov) satellite imagery reveals frequent occurrences of island vortex streets in many parts of the world, particularly those regions where frontal, subsidence, or radiation inversions provide the stability required for flow blocking. These vortex streets are produced most often by Jan Mayen Island (Mohr 1971; Scorer 1986), Guadalupe (Chopra 1973), the Canary Islands (Hubert and Krueger 1962; Chopra 1973), Cheju (Tsuchiya 1969; Chopra 1973; Jensen and Agee 1978), the Aleutian Islands (Thomson et al. 1977), Madeira (Chopra and Hubert 1965; Moll 1971; Chopra 1973), the Cape Verde Islands (Chopra 1973), and Reunion (Chopra 1973). Figure 1 is an example of a typical atmospheric vortex street; in this case it formed in the wake of Guadalupe at 1845 UTC 13 June 2004. A quantitative analysis of this, and similar imagery from 29 other cases from around the world, is conducted here with the ob-

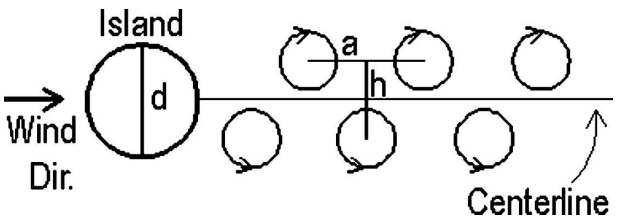

FIG. 2. A schematic diagram of a mountainous island of crosswind width d and its von Kármán vortex street showing the cross-street distance h and the along-street distance a between two like-rotating vortices.

jective of characterizing the geometry of these vortex streets and relating it to existing similarity theory. Qualitative analysis of these images provides observational support for recent three-dimensional modeling results.

Given the 250-m resolution of the *Terra* and *Aqua* MODIS satellites, it is now possible to measure the spacing of individual von Kármán vortices with a precision 4 times better than that provided by NOAA or Geostationary Operational Environmental Satellites (Hansen et al. 2003). For this study, the National Aeronautics and Space Administration's (NASA's) archived collection of MODIS images was examined to find 30 well-defined cases of island wakes with the multiple alternately rotating vortices (e.g., Fig. 1) of a vortex street. Photogrammetric methods are then applied to obtain the crosswind diameter of the island d, the along-street distances between adjacent like-rotating vortices a, and the cross-street distance between adjacent oppositely rotating vortices h (Fig. 2). These measurements are used to test the applicability of existing similarity theory to atmospheric vortex street geometry. This is done by calculating, from imagery, the dimensionless ratios describing vortex geometry: the aspect ratio

$$a/h \tag{1}$$

and the dimensionless width

$$h/d. \tag{2}$$

The distribution of these observed ratios is then compared with the values developed in the theoretical and numerical studies of von Kármán and Rubach (1912), Tyler (1930), and Schär and Smith (1993a,b).

Vortex streets behind bluff bodies have been studied theoretically using inviscid stability analysis (von Kármán and Rubach 1912) and direct experimentation (e.g., Tyler 1930; Tritton 1988, chapter 3), along with numerous numerical simulations (e.g., Mohensi 2000). Likewise, numerical simulation of island wakes has been undertaken by Smolarkiewicz and Rotunno (1989), Rotunno and Smolarkiewicz (1991), Schär and Smith (1993a,b), Schär and Durran (1997), and Epifanio and Durran (2002a,b). Although island-generated vortex streets have been simulated successfully by Schär and Smith (1993a) and Epifanio and Durran (2002a,b), robust observational tests of the applicability of bluff body vortex street geometric similarity theories to such atmospheric flow has awaited the availability of high-resolution visible satellite imagery.

The studies discussed above indicate that flow blocking is an essential element of island vortex street formation, so two dimensionless controlling parameters are suggested, the Froude number and the dimensionless mountain height. For a shallow-water system, such as was studied by Schär and Smith (1993a,b), the Froude number F_∞ is given by

$$F_\infty = \frac{U_\infty}{\sqrt{gH_\infty}}, \tag{3}$$

where U_∞ is the upstream velocity, g is the acceleration of gravity, and H_∞ is the fluid depth well upstream of the mountain. The dimensionless mountain height M is given by the mountain height to fluid depth ratio

$$M = \frac{h_m}{H_\infty}, \tag{4}$$

where h_m is the mountain height. For continuously stratified flow such as that studied by Schär and Durran (1997), the corresponding formulas are no longer independent:

$$F_\infty = \frac{U_\infty}{Nh_m} \tag{5}$$

and

$$M = \frac{1}{F_\infty}, \tag{6}$$

where

$$N = \sqrt{\frac{g}{\theta_v}\frac{\partial \theta_v}{\partial z}} \tag{7}$$

is the Brunt–Väisälä frequency.

The stability profile is more complex for the inversion-capped stratocumulus environments where atmospheric vortex streets are observed. The stratocumulus lies within an unstable boundary layer and is capped by the subsaturated air of a strong inversion (e.g., Jensen and Agee 1978; Etling 1989). When early researchers noted that island wakes formed in association with a stable lid over an unstable boundary layer, they often surmised that the vortices existed primarily within the capping inversion. More recent studies of stratocumu-

lus (e.g., Jensen and Agee 1978; Etling 1989) show that the stratocumulus is confined to the unstable boundary layer below this inversion, so the vortices observed in these clouds must, at the very least, extend down into the boundary layer. In support, synthetic aperture radar observations reveal the stress patterns of these vortices on the ocean surface (e.g., Li et al. 2000) indicating that they can span the depth of the boundary layer. The generation mechanism for atmospheric vortex streets must therefore be applicable to this situation of a mixed layer trapped under a strong, but deformable inversion.

Understanding of this vorticity generation mechanism has evolved along with understanding of the stability profile in stratocumulus-topped boundary layers and the combination of three-dimensional and quasi-two-dimensional flow that results. Hubert and Krueger (1962) suggest that atmospheric vortex streets could not be composed of mechanical eddies because their longevity was incompatible with the downscale energy cascade in three-dimensional turbulence. This argument becomes irrelevant when one considers the large diameter-to-depth ratio of each vortex, and simulation results indicating that they are quasi-two-dimensional balanced vortices (e.g., Schär and Durran 1997).

The next hypothesis, put forward by Chopra and Hubert (1965) and Chopra (1973), was that atmospheric vortex streets draw their vorticity from separation of the viscous boundary layer of the island, much as in flow around the bluff body. Jensen and Agee (1978) review the dynamics of this process. Etling (1989) explicitly states, however, that there may be other mechanisms for wake formation besides boundary layer flow separation, noting the importance of the Froude number in determining the dimensionality of flow past an isolated island. He provides a formulation for the dividing streamline height h_c, which highlights the capping inversion as a likely location because of its great contribution to the integrated stability,

$$\frac{1}{2}\,U^2(h_c) = \int_{h_c}^{h_m} N^2(z)(h_m - z)\,dz. \tag{8}$$

Three-dimensional laboratory studies of stratified flow reviewed by Etling (1989) suggest that $h_c > 0.6h_m$ is required for vortex street formation. This result suggests that three-dimensional flow over a mountain is required for the formation of atmospheric vortex streets, and that the boundary layer shedding is not sufficient.

Laboratory studies of stratified flow over a cone (e.g., Boyer et al. 1987) support this view, with the theory being refined through a series of carefully crafted runs using partial-physics numerical models, wherein the successes and failures both provide insight into which processes were necessary or merely sufficient. Dempsey and Rotunno (1988) show that two-dimensional (i.e., mixed layer) models can generate lee vortices only by boundary layer shedding (i.e., flow separation). In contrast, Smolarkiewicz and Rotunno (1989) and Rotunno and Smolarkiewicz (1991) show that three-dimensional models can do so with no surface friction and hence no boundary layer to be shed. Instead, baroclinic generation of vorticity results from the horizontal buoyancy gradients created by deformation of isentropic surfaces during flow over the island. Schär and Durran (1997) extend this result from vortex pairs to vortex streets while Schär and Smith (1993a) obtain similar results with a shallow-water model, again with no surface friction.

The importance of mountain wave formation to this baroclinic generation of vorticity is highlighted by Smolarkiewicz and Rotunno (1989), Schär and Smith (1993a), and Schär and Durran (1997). This wave explains leeside clearing observed in satellite images (e.g., Fig. 1) as the result of subsidence as well as the turbulent mixing postulated by Lyons and Fujita (1968). The mountain wave plays a second role, in which wave steepening and breaking (Smolarkiewicz and Rotunno 1989) are required to obtain flow reversal in lee of the island. Epifanio and Durran (2002a) using a three-dimensional nonhydrostatic free-slip model note that this breaking wave looks much like the hydraulic jump seen in shallow-water calculations of Schär and Smith (1993a), despite being phenomenon of continuously stratified flow. They note that while the gradient of buoyancy across the jump directly contributes to flow reversal, the vertical vorticity generated by the jump is opposed to that created by the processes described above.

Recent studies have highlighted several different processes at work within the jump. Schär and Durran (1997) and Epifanio and Durran (2002a,b) note that numerical diffusion and turbulence closure can play a role in breaking waves or hydraulic jumps and that neither are wholly physical, so caution is required in interpreting this aspect of any numerical result. While this includes much of the vorticity generation in the jumps, Epifanio and Durran (2002a,b) obtain similar results with two different closures suggesting some robustness.

Thus, a number of processes contribute to the creation of vortices in the lee of mountainous islands. Vorticity budget calculations show that vorticity is first generated baroclinically as a result of isentrope tilting in the mountain wave upwind of the jump. This vorticity is then stretched in the jump (with mixing effects possibly

contributing), and advected downwind off the ends of the jump [see Fig. 4 of Epifanio and Durran (2002a) for description and Fig. 3 in Epifanio and Durran (2002b) for dynamics].

Thus, the island wake sidewalls are shear lines extending downstream from the ends of a hydraulic jump or breaking wave (Chopra 1973; Schär and Smith 1993a; Epifanio and Durran 2002a,b). Schär and Smith (1993b) and Schär and Durran (1997) show how vortex streets can form by positive feedback between perturbations located on these two shear lines. The embedding of the vortices in a slow wake is noted by Tsuchiya (1969) using satellite cloud tracking and is supported by all of the theoretical studies discussed above. The slow wake can also be expressed in terms of a Bernoulli deficit (Schär and Smith 1993a; Schär and Durran 1997; Epifanio and Durran 2002a,b), or in terms of potential vorticity production.

Shallow-water models predict potential vorticity production by dissipation in the hydraulic jump (Schär and Smith 1993a) but it requires a three-dimensional study to determine the mechanism (Schär and Durran 1997). Potential vorticity is conserved in an inviscid adiabatic fluid (Smolarkiewicz and Rotunno 1989), but the fluid has neither property if there is a breaking wave or hydraulic jump. Thus, potential vorticity can be created by thermal dissipation (i.e., mixing) in the jump (Epifanio and Durran 2002b) while momentum mixing opposes this effect. Potential vorticity generation is strongest at the lateral edges and somewhat downwind of the jump from which point it advects downstream in the shear lines at the sides of the wake (Smolarkiewicz and Rotunno 1989; Epifanio and Durran 2002b). Schär and Durran (1997) show different dissipation mechanisms can yield potential vorticity generation depending on the dimensionless mountain height: wave breaking for short mountains (high dividing streamline), or dissipation in the wake for tall mountains (low dividing streamline). They also note that the modeled forms are independent of initial conditions, supporting the feature robustness observed in the continuously evolving atmosphere. Moreover, although potential vorticity is greatest above the jump's well-mixed wake, vorticity is greatest within the wake, as expected from the observation of vortices in stratocumulus (Schär and Durran 1997).

Visible manifestations of vortex streets in stratocumulus support many of the features seen in these two- and three-dimensional models. A clear eye is frequently observed in the vortex center (e.g., Fig. 1 and Chopra 1973). This suggests either warming and drying of the boundary layer by entrainment or lowering of the inversion to a height below the lifting condensation level of the boundary layer. Hubert and Krueger (1962) speculate that the low pressure required for vortex circulation is produced by such inversion lowering. Model results from Schär and Durran (1997) support this view. As Fig. 1 shows, the eye typically fills in as the vortex drifts downstream, suggesting that the inversion gradually returns to its original level. This filling is a natural consequence of the convergence into a frictionally damped vortex (Hubert and Krueger 1962; Chopra and Hubert 1965). Thus, the satellite imagery of vortex decay is consistent with the evolution of a warm-core vortex caused by the local depression of the capping inversion. The spiral cloud patterns sketched by Chopra and Hubert (1965) and shown by (Chopra 1973) could be the result of this inflow. They could also result from vortex deformation of preexisting mesoscale cellular convection, or by some internal secondary circulation within the vortex. The outer cloud band of these spirals often link to bracket a pair of adjacent counterrotating vortices (Chopra and Hubert 1965; Jensen and Agee 1978). A similar pattern can be seen in the confluence lines of Fig. 1 in Schär and Durran (1997) and in the bands of elevation in potential temperature surfaces in Fig. 16 therein.

The aspect ratio of vortex streets has been studied extensively in both the atmosphere and laboratory. The ratio of the cross-street distance between two halves of the vortex street h to the along-street distance between two adjacent like-rotating vortices a has a value of 0.28 for the inviscid theory of von Kármán and Rubach (1912). In contrast, Chopra and Hubert (1965) derive a value of 0.39 using a drag-based theory. They quote laboratory studies yielding values ranging from 0.28 to 0.52 depending on the shape of the body, flow characteristics, and distance downstream. Atmospheric values for small sample case studies include 0.43 for one image of Madeira (Chopra and Hubert 1965), 0.332 from several images of Cheju (Tsuchiya 1969), 0.5 from two images of Cheju (Jensen and Agee 1978), and 0.38–0.60 for one image of the Aleutian chain (Thomson et al. 1977). The dimensionless width has been studied less extensively, with Hubert and Krueger (1962) stating that it approximates 1 for island wakes while Tyler (1930) reported a value of 1.2 for a bluff body laboratory flow.

Horizontal eddy diffusivity has been implicated in the bias toward larger aspect ratios in the turbulent flow (Chopra and Hubert 1965; Chopra 1973). Studies of this effect, including Abernathy and Kronauer (1962), Mair and Maull (1971), and Papailiou and Lykoudis (1974), were reviewed by Thomson et al. (1977). Chopra and Hubert (1965) used von Kármán vortex street theory to diagnose the horizontal eddy diffusivity

from observed vortex lifetimes. The value was fairly large, around 4000 $m^2 s^{-1}$, perhaps a result of the mesoscale cellular convection within which their vortices were embedded.

This study focuses on two of the geometric parameters of atmospheric vortex streets, the aspect ratio and the dimensionless width. Since the model of Schär and Smith (1993b) confirms the inviscid theoretical result of von Kármán and Rubach (1912), the aspect ratio value of 0.28 will be used as a null hypothesis in the statistical evaluation of our 30-image sample of atmospheric vortex streets. Likewise, the null hypothesis for the dimensionless width is that for a bluff body, approximately 1.2 according to the laboratory results of Tyler (1930).

The MODIS satellite images, and the criterion used to select vortex street cases, are described in section 2. The procedures used to determine the vortex center positions and to calculate the two similarity ratios are described in section 3. The quantitative results of this analysis are presented, tested against theory, and discussed in section 4. A summary of the observations and results is presented in section 5, along with conclusions about the impact of boundary layer turbulence on atmospheric vortex streets.

2. Data

This observational study is based on a 30-case sample of MODIS satellite images of well-developed vortex streets. These images come from the multiyear archive of images of the *Terra*/*Aqua* MODIS satellite provided by NASA. The MODIS satellites are polar orbiting at an altitude of 705 km, have a swath width of approximately 2300 km, and provide full color visible images. Each image is provided at a resolution of 4 km, 2 km, 1 km, 500 m, and 250 m. The 250-m-resolution images are used in this study so that the distances and dimensionless ratios could be computed with maximum possible precision. To minimize the impact of parallax distortion on the photogrammetric distance calculations (Thomson et al. 1977), only those images with vortices within the center third of the pixel swath are analyzed. This restriction kept the off-nadir viewing angles to less than 28°, yielding a maximum along-street to cross-street distortion of at most 12%. Because the cases are distributed across this central third of the image swath, the average off-nadir angle is half of this threshold value, resulting in an average distortion of approximately 3%, a value roughly equivalent to the accuracy to which the intervortex distances can be computed at nadir using the 250-m-resolution MODIS imagery. Moreover, the distortion could be of either sign depending on the orientation of the vortex street relative to the satellite ground track, and so the results reported below are biased by an even smaller value.

To analyze only atmospheric cases corresponding to the simple, unsheared uniform flow studied by von Kármán and Rubach (1912), a set of criteria are applied to select the 30 vortex street images for this study. Only mature-stage cases exhibiting a vortex street that extends well beyond the immediate wake of the island are used, thereby eliminating the other vortex-pair wake regime also reported by Schär and Smith (1993a,b) and Schär and Durran (1997). Moreover, cases in which cross-flow shear of the mean flow damped vortices with one sign of rotation relative to those of the other are excluded from the sample, because the theoretical, modeling, and laboratory studies assume uniform upwind flow. To obtain robust statistics, each usable vortex street is required to contain at least four vortices. This minimum number allows the vortex street centerline to be computed so that the intervortex distances could be separated into along-street and cross-street components, as described below. The actual vortex number ranges from 4 to 14, with a median of 6 vortices. Most cases have a linear vortex street centerline, indicating a steady wind direction over the previous few hours. Cases in which the centerline of the vortex street is curved, reflecting a gradual change in the synoptic wind direction with space or time, are also analyzed through a different procedure in which a polynomial curve is used to fit the centerlines described in section 3.

3. Procedures

Use of the criterion presented in section 2 produces 30 images of island wake vortex streets that could be analyzed quantitatively, with the goal of determining the two dimensionless ratios that describe vortex size and the vortex spacing within the vortex street. The GNU image manipulation program (GIMP; http://www.gimp.org/) is used to determine the vortex center positions from which the street centerlines and the intervortex distances are then computed. The pixel coordinates for each vortex are taken to be those for the center toward which its cloud spiral converged. Distances between vortices are then computed in pixels and converted to kilometers using the satellite pixel resolution of 250 m. Two components of the distance between adjacent vortices that are required for the subsequent analysis are the along-street distance a and the cross-street distance h, as shown in Fig. 2. For each of these measurements, and for the resulting aspect ratios and dimensionless width ratios, the mean, standard deviation, and coefficient of variation (standard deviation divided by mean) are computed across the 30-case

TABLE 1. The mean, std dev, coef of variation, probability of acceptance of the null hypothesis, 95% confidence interval, and hypothesis test results for the track aspect ratio and dimensionless width ratio without the inclusion of curvature.

	Mean	Std dev	COV	Probability	95% confidence interval	Hypothesis test result
Aspect ratio	0.42	0.019	0.045	1.78×10^{-5}	0.36, 0.47	Reject
Dimensionless width ratio	1.61	1.04	0.64	0.038	1.23, 2.00	Reject

sample. The crosswind width d of the island responsible for the vortex street is determined by computing the distance between two coastal coordinates, one on each side of the island. This approach may have yielded an overestimate of the obstacle diameter as the island flanks were sloped rather than vertical (Chopra and Hubert 1965).

To account for possible vortex street curvature, three centerlines (Fig. 2) are found for each of the 30 cases. The first centerline is determined by calculating a best-fit line to the points located midway between each adjacent pair of vortex centers. This method works well and is unbiased for straight vortex streets having at least three vortices, but breaks down if vortex streets curve. The second centerline was also a linear best fit obtained in this manner, but the first vortex in the vortex street is excluded because its position might be perturbed by its recent separation from the island. The use of this method imposed the four-vortex minimum vortex street length noted above. A third vortex street centerline is also linear, but uses an analyst-defined line. This visual estimate is used solely as a check on the objective procedures. The objective centerline having the least squared error is used for the intervortex distance measurement. If both vortex centerlines yield identical squared error values, then the centerline based on all of the vortices is used.

There are a few cases among the 30 that exhibit some curvature between the start and end point of the island vortex street. Rather than using a linear centerline for these cases, a least squares optimization is applied to fit polynomial functions to the intervortex center points. These functions are then graphed for quality control, and a squared error fit score calculated to determine which order polynomial is most appropriate for each curved vortex street. Second- and third-order polynomials are tested in each case, and the best was selected for use as the curved centerline. The order of the polynomial is limited to three to prevent the function from fitting minor wobbles in vortex position that should be treated instead as error in similarity theory.

The resulting intervortex distances, a and h, and crosswind width of the island d for each case are used to compute the two dimensionless ratios of interest, Eqs. (1) and (2) in the introduction. As stated above, the aspect ratio is the dimensionless ratio of the cross-street distance between adjacent oppositely restating vortices, h, to the along-street distance between two like-rotating vortices, a. The other dimensionless ratio determined for the vortex streets was the dimensionless width, the ratio of the cross-street distance between adjacent vortices to island's cross-street width. Thus, the dimensionless width quantifies the relationship between the island's size and the vortex street width. The means for the along-street and cross-street intervortex, distances are found for each vortex street, and these mean values of a and h are then used to compute the aspect ratio and width ratio for that vortex street.

The 30-case sample of observed values of these two dimensionless ratios is then compared with laboratory and theoretical values from previous studies. For this comparison, one-sample t tests (Wilks 1995) are performed on the values determined from the satellite images against null hypotheses based on the theoretical values. The null hypothesis for the aspect ratio is von Kármán's value for inviscid flow around a cylinder, 0.28 (Schär and Smith 1993b). The null hypothesis for the dimensionless width ratio is 1.2, the value determined by Tyler (1930) for a bluff body, and verified by photogrammetric analysis of the model results shown in Mohensi (2000).

These hypothesis tests are performed for both the linear and curved centerline datasets, eliminating the potential bias that may have been induced in the results by over- or underfitting the vortex street centerlines. These two sets of hypothesis test results are compared to determine the impact of the vortex street curvature on the statistically based conclusions.

4. Results

The result of the one-sample t test of the aspect ratio computed using linear centerlines is to reject the null hypothesis value of 0.28 at the 95% confidence level (Table 1). The probability of accepting the von Kármán inviscid aspect ratio is actually much less than 1%. The 95% confidence interval determined from the statistical test is between 0.36 and 0.47, with a mean value of 0.42. Thus, for the atmospheric vortex streets in the wake of a mountainous island, the aspect ratio will most likely fall in the relatively narrow range between those two numbers; the narrowness of this confidence interval,

TABLE 2. The mean, std dev, coef of variation, probability of acceptance of the null hypothesis, 95% confidence interval, and hypothesis test results for the track aspect ratio and dimensionless width ratio with the inclusion of curvature.

	Mean	Std dev	COV	Probability	95% confidence interval	Hypothesis test result
Aspect ratio	0.37	0.019	0.052	8.7×10^{-3}	0.30, 0.43	Reject
Dimensionless width ratio	1.83	1.15	0.63	0.0057	1.40, 2.25	Reject

reflected in the coefficient of variation of less than 5%, indicates that the geometric similarity is valid for the atmospheric vortex streets, despite the statistically significant difference in the similarity constant. It is noteworthy that the scatter in this set of aspect ratio observations is much smaller than that between previously reported cases from this same set of islands. The improvement in performance of this geometric similarity probably results from the much larger set of potential cases available in the MODIS archive, which allowed selection of a set of well-defined cases with large vortex counts. In contrast, pervious investigators had to make do with a much more limited sample of cases, with case selection dictated more by image availability than quality.

The statistically significant difference in the aspect ratio compared with inviscid theory is expected given the conditions in which atmospheric vortex streets form. The von Kármán aspect ratio was derived for inviscid, neutrally stratified laboratory flow around a cylinder. In contrast, the island wake vortices generally form in a highly viscous and stratocumulus-filled boundary layer having unstable stratification below a capping inversion. As noted by Chopra and Hubert (1965), Chopra (1973), and Thomson et al. (1977) horizontal eddy viscosity could be expected to expand the vortices with time and thus increase the value of the aspect ratio similarity constant. Moreover, laboratory studies suggest that vortex street structure can be changed by a spatial and temporal variation in the upstream winds, a real possibility in the atmosphere of the earth (Mohensi 2000).

The results for the dimensionless width ratio compared using linear centerlines suggest that the cross-street offset between adjacent vortex centers is indeed proportional to the cross-wind island diameter as suggested by existing geometric similarity theory. The one-sample *t* test performed on the dimensionless width versus the null hypothesis value of 1.2 yields a probability value of 0.038, allowing rejection of the theoretical value at the 95% confidence level. The 95% confidence interval for the dimensionless width ratio is 1.23 to 2.0, with a mean value of 1.61. Thus, although the test rejected the null hypothesis value of 1.2, there is still a moderately strong relationship between the crosswind diameter of the island and the cross-street distance between adjacent vortices. The increased vortex diameter compared with inviscid theory can again be linked to vorticity diffusion by boundary layer turbulence. In the 30 cases used for this study, the vortex spread is observed to increase downwind, consistent with such turbulent diffusion. Thus, the width ratio, for shorter cases having fewer vortices, would be expected to be in closer agreement with the null hypothesis of 1.2, and longer vortex streets may be skewed from this number by the ongoing effects of boundary layer eddy viscosity.

The above conclusions are formulated using the distances found for linear centerlines. The same statistical tests also are performed on the data computed using the curved vortex centerlines in those cases where they yielded a better fit. These results are presented in Table 2. The results are statistically similar to those obtained using linear centerlines. The resulting aspect ratio, although closer to the null hypothesis value of 0.28, is still rejected at the 95% confidence level, the probability of acceptance having increased only to 0.0087. Likewise, the upper and lower bounds of the 95% confidence interval are lowered. The coefficient of variation increased to a bit over 5%, suggesting that the similarity theory may explain slightly less of the variation than would be suggested by the linear centerline analysis. The probability of acceptance for the dimensionless width is lowered from 0.038 for the linear centerline test to 0.0057 for the test including the curved centerlines, and so the null hypothesis of the dimensionless width is still rejected at the 95% confidence level. Likewise, the coefficient of variation decreases slightly, suggesting that the similarity is at least as strong as suggested by the simple linear centerline analysis. As seen for the aspect ratio, however, the upper and lower bound of the 95% confidence interval is lowered.

5. Conclusions

An observational analysis of 30 observed island wake vortex streets reveals, through statistical tests, that von Kármán's inviscid aspect ratio is a somewhat biased approximation of the value for atmospheric vortex streets, although the geometric similarity theory does collapse the data (i.e., the variance in the dimensionless ratio is much less than that of the parameters from which it is composed). The observed mean value of

0.418 is larger than the inviscid value of 0.28 at the 95% significance level. This difference is expected, as these atmospheric vortices do not occur in the inviscid, neutrally stratified conditions assumed by von Kármán. The atmospheric flow is viscous as a result of an interaction with the terrain and the existence of convective and shear-induced turbulence in the stratocumulus-topped boundary layer. Moreover, flow upwind of these islands is not uniform; speed and direction in the atmosphere do vary, potentially causing deformation of the flow and thus distortion of the structure of the island wake vortices.

Based on this sample of 30 cases, a more realistic aspect ratio (cross-street distance between adjacent oppositely rotating vortices divided by the along-street distance between adjacent like-rotating vortices) has a mean value of 0.42 and a 95% confidence interval of 0.36–0.47. Likewise, an analysis of the connection between the island width and the cross-street diameter leads to the laboratory value of 1.2 (Tyler 1930) barely being rejected at the 95% confidence level. Despite the rejection of the theoretical value of this dimensionless constant, the island width does explain much of the variation in the vortex street width, supporting the validity of the geometric similarity theory. Cases in which the elevated terrain has a lesser diameter than the island itself may contribute to both bias and scatter in the atmospheric datasets compared with laboratory theory. Dropsonde observations of the upwind boundary layer depth would be required to determine the island diameter at inversion base and thus the extent to which that parameter is a better predictor of vortex street width. A further complication is that the vortex street width often increases and the vortices spread out as they drift downwind, suggesting the same diffusive effects seen in the aspect ratio.

Acknowledgments. The authors extend their thanks to the Summer Experience in Earth and Mineral Sciences team of Ashley Diggs, Susan Jacob, Samuel Burlacu, Francisco Martinez, and Shane Gallup for their contributions to the development and testing of the quantitative MODIS satellite image analysis techniques used in this study and to Dr. Hampton Shirer and the anonymous reviewers for valuable suggestions on vortex street dynamics.

REFERENCES

Abernathy, F. H., and R. E. Kronauer, 1962: The formation of vortex streets. *J. Fluid Mech.,* **13,** 1–20.

Boyer, D. L., P. A. Davies, W. R. Holland, and F. Honji, 1987: Stratified rotating flow over and around isolated theedimensional topography. *Philos. Trans. Roy. Soc. London,* **322A,** 213–241.

Chopra, K. P., 1973: Atmospheric and oceanic flow problems introduced by islands. *Advances in Geophysics,* Vol. 16, Academic Press, 297–421.

——, and L. F. Hubert, 1965: Mesoscale eddies in wakes of islands. *J. Atmos. Sci.,* **22,** 652–657.

Dempsey, D. P., and R. Rotunno, 1988: Topographic generation of mesoscale vortices in mixed-layer models. *J. Atmos. Sci.,* **45,** 2961–2978.

Epifanio, C. C., and D. R. Durran, 2002a: Lee-vortex formation in free-slip stratified flow over ridges. Part I: Comparison of weakly nonlinear inviscid theory and fully nonlinear viscous simulations. *J. Atmos. Sci.,* **59,** 1153–1165.

——, and ——, 2002b: Lee-vortex formation in free-slip stratified flow over ridges. Part II: Mechanisms of vorticity and PV production in nonlinear viscous wakes. *J. Atmos. Sci.,* **59,** 1166–1181.

Etling, D., 1989: On atmospheric vortex streets in the wake of large islands. *Meteor. Atmos. Phys.,* **41,** 157–164.

Hansen, M. C., R. S. DeFries, J. R. G. Townshend, M. Carroll, C. Dimiceli, and R. A. Sohlberg, 2003: Global percent tree cover at a spatial resolution of 500 meters: First results of the MODIS vegetation continuous fields algorithm. *Earth Interactions,* **7.** [Available online at http://EarthInteractions.org.]

Hubert, L. F., and A. F. Krueger, 1962: Satellite pictures of mesoscale eddies. *Mon. Wea. Rev.,* **90,** 457–463.

Jensen, N. O., and E. M. Agee, 1978: Vortex cloud street during AMTEX 75. *Tellus,* **30,** 517–523.

King, M. D., and Coauthors, 2003: Cloud and aerosol properties, precipitable water, and profiles of temperature and humidity from MODIS. *IEEE Trans. Geosci. Remote Sens.,* **41,** 442–458.

——, S. Platnick, P. Yang, G. T. Arnold, M. A. Gray, J. C. Riedi, S. A. Ackerman, and K.-N. Liou, 2004: Remote sensing of liquid water and ice cloud optical thickness and effective radius in the Arctic: Application of airborne multispectral MAS data. *J. Atmos. Oceanic Technol.,* **21,** 857–875.

Li, X., P. Clemente-Colon, W. G. Pichel, and P. W. Vachon, 2000: Atmospheric vortex streets on a RADARSAT SAR image. *Geophys. Res. Lett.,* **27,** 1655–1658.

Lyons, W. A., and T. Fujita, 1968: Mesoscale motions in oceanic stratus as revealed by satellite data. *Mon. Wea. Rev.,* **96,** 304–314.

Mair, W. A., and D. J. Maull, 1971: Bluff bodies and vortex shedding—A report on Euromech 17. *J. Fluid Mech.,* **45,** 209–224.

Mohensi, K., 2000: Studies of two-dimensional vortex streets. *Proc. 31st AIAA Fluid Dynamics Conf. and Exhibition,* Anaheim, CA, AIAA, 1–9.

Mohr, T., 1971: Karman-Wirbel im Lee von Jan Mayern. *Meteor. Rdsch.,* **24,** 30–32.

Moll, H. G., 1971: Die atmosphäriche Umströmung Madeiras. *Contrib. Atmos. Phys.,* **44,** 227–244.

Papailiou, D. D., and P. S. Lykoudis, 1974: Turbulent vortex streets and the entrainment mechanism of the turbulent wake. *J. Fluid Mech.,* **62,** 11–31.

Platnick, S., M. D. King, S. A. Ackerman, W. P. Menzel, B. A. Baum, J. C. Riédi, and R. A. Frey, 2003: The MODIS cloud products: Algorithms and examples from *Terra. IEEE Trans. Geosci. Remote Sens.,* **41,** 459–473.

Rotunno, R., and P. K. Smolarkiewicz, 1991: Further results on lee vortices in low-Froude-number flow. *J. Atmos. Sci.,* **48,** 2204–2211.

Schär, C., and D. R. Durran, 1997: Vortex formation and vortex shedding in continuously stratified flows past isolated topography. *J. Atmos. Sci.,* **54,** 534–554.

——, and R. B. Smith, 1993a: Shallow-water flow past isolated topography. Part I: Vorticity production and wake formation. *J. Atmos. Sci.,* **50,** 1373–1400.

——, and ——, 1993b: Shallow-water flow past isolated topography. Part II: Transition to vortex shedding. *J. Atmos. Sci.,* **50,** 1401–1412.

Scorer, R., 1986: *Cloud Investigations by Satellite*. Ellis Horwood, 300 pp.

Smolarkiewicz, P. K., and R. Rotunno, 1989: Low Froude number flow past three-dimensional obstacles. Part I: Baroclinically generated lee vortices. *J. Atmos. Sci.,* **46,** 1154–1164.

Thomson, R. E., J. F. R. Gower, and N. W. Bowker, 1977: Vortex streets in the wake of the Aleutian Islands. *Mon. Wea. Rev.,* **105,** 873–884.

Tritton, D. J., 1988: *Physical Fluid Dynamics.* 2d ed. Oxford University Press, 591 pp.

Tsuchiya, K., 1969: The clouds with the shape of Kármán vortex street in the wake of Cheju Island, Korea. *J. Meteor. Soc. Japan,* **47,** 457–465.

Tyler, J., 1930: A hot wire method for measurement of the distribution of vortices behind obstacles. *Philos. Mag.,* **11,** 489–490.

von Kármán, T., and H. Rubach, 1912: Über den mechanismus des flüssigkeits—und luftwiderstandes. *Phys. Z.,* **13,** 49–59.

Wilks, D. S., 1995: *Statistical Methods in the Atmospheric Sciences*. Academic Press, 464 pp.

Zimmerman, L. I., 1969: Atmospheric wake phenomena near the Canary Islands. *J. Appl. Meteor.,* **8,** 896–907.